Vol. 36 – N° 1 03 12 p. 61 – 73

GEOSTANDARDS and GEOANALYTICAL RESEARCH

Chemical Characterisation of Natural Ilmenite: A Possible New Reference Material

Patrick H. **Donohue***, Antonio **Simonetti** and Clive R. **Neal**

Department of Civil Engineering and Geological Sciences, 156 Fitzpatrick Hall, University of Notre Dame IN 46556, USA
* Corresponding author. e-mail: pdonohu1@nd.edu

Seven ilmenite ($FeTiO_3$) megacrysts derived from alnöite pipes (Island of Malaita, Solomon Islands) were characterised for their major and trace element compositions in relation to their potential use as secondary reference materials for *in situ* microanalysis. Abundances of thirteen trace elements obtained by laser ablation ICP-MS analyses (using the NIST SRM 610 glass reference material) were compared with those determined by solution-mode ICP-MS measurements, and these indicated good agreement for most elements. The accuracy of the LA-ICP-MS protocol employed here was also assessed by repeated analysis of MPI-DING international glass reference materials ML3B-G and KL2-G. Several of the Malaitan ilmenite megacrysts exhibited discrepancies between laser ablation and solution-mode ICP-MS analyses, primarily attributed to the presence of a titano-magnetite exsolution phase (at the grain boundaries), which were incorporated solely in the solution-mode runs. Element abundances obtained by LA-ICP-MS for three of the ilmenite megacrysts (CRN63E, CRN63H and CRN63K) investigated here had RSD (2*s*) values of ‹ 20% and therefore can be considered as working values for reference purposes during routine LA-ICP-MS analyses of ilmenite.

Keywords: *in situ* analysis, ilmenite, laser ablation, ICP-MS, analytical techniques, reference material.

Sept méga cristaux d'ilménite ($FeTiO_3$) provenant de pipes d'alnoïte (île de Malaita, Iles Salomon) ont été caractérisés en termes de compositions en éléments majeurs et traces pour appréhender leur potentiel en vue d'une utilisation comme matériaux de référence secondaires pour la microanalyse in situ. Les abondances de treize éléments traces obtenues par la méthode LA-ICP-MS (en utilisant le verre NIST SRM 610 comme matériel de référence) ont été comparées avec celles déterminées par la technique solution ICP-MS. Cette comparaison met en évidence un bon accord des résultats pour la plupart des éléments. La précision du protocole LA-ICP-MS utilisé a également été évaluée par l'analyse répétée des verres de référence internationaux MPI-DING ML3B-G et KL2-G. Plusieurs des mégacristaux d'ilménite de Malaita montrent des divergences entre les résultats obtenus par LA-ICP-MS et par solution ICP-MS, divergences principalement attribuables à la présence d'exsolutions de titano-magnétite (aux joints de grains), exsolutions qui sont prises en compte uniquement par la technique solution ICP-MS. Les abondances des éléments obtenus par LA-ICP-MS pour trois des mégacristaux d'ilménite (CRN63E, CRN63H et CRN63K) étudiés ici avaient des déviations standards relatives (RSD, 2s) de moins de 20%, et peuvent donc être considérés comme des valeurs de travail utilisables à des fins de référence lors de l'analyse LA-ICP-MS en routine de l'ilménite.

Mots-clés : analyse in situ, ilménite, ablation laser, ICP-MS, techniques analytiques, matériaux de référence.

Received 11 Nov 10 – Accepted 09 May 11

Ilmenite is a common accessory mineral in igneous and metamorphic rocks and is a major constituent in terrestrial rocks of cumulate origin and high-titanium lunar basalts (e.g., Papike *et al.* 1976, Mitchell 1977, Moore *et al.* 1992, Charlier *et al.* 2007), the latter containing › 15 modal per cent ilmenite (e.g., Brown *et al.* 1975, Warner *et al.* 1975, 1978). Ilmenite is an early and prolonged liquidus phase in high-Ti lunar basalts, generally crystallising

doi: 10.1111/j.1751-908X.2011.00124.x

after olivine and armalcolite (Dymek *et al.* 1975, Papike *et al.* 1976, Stanin and Taylor 1979). Moreover, ilmenite is an important megacryst and groundmass phase in kimberlites (e.g., Moore *et al.* 1992, Mitchell 1977). Ilmenite incorporates elements that are considered both compatible (Cr, V, Ni) and incompatible (Zr, Nb) in silicate minerals, which in conjunction with its prolonged crystallisation interval may record changes in melt chemistry and crystal fractionation processes.

Despite its importance for petrological investigations, there is no well-characterised, matrix-matched reference material available for the validation of results obtained from high spatial resolution analysis of ilmenite. Matrix matching of a reference material to unknown samples is key in reducing matrix-dependent ionisation effects in a plasma environment, including analytical errors associated with varying ionisation energy, viscosity (for solution-mode analyses) and relative concentrations of elements. Early ilmenite analysis techniques via electron microprobe (EPMA) focused on a selected group of trace elements (e.g., Cr, V, Zr and Nb; El Goresy *et al.* 1971, McCallum and Charette 1978), or relied on doping of experimental products to bring concentrations to percent levels for measurement by EPMA (McKay *et al.* 1986, Nakamura *et al.* 1986). Few previous investigations have analysed ilmenite for their trace element abundances via the *in situ* laser ablation-inductively coupled plasma-mass spectrometry (LA-ICP-MS) method. One example is the comprehensive determination of trace elements in synthetic ilmenite by Klemme *et al.* (2006), which utilised titanium as the internal standard and the NIST SRM 610 glass as the calibrator.

The NIST SRM 610 and 612 glass reference materials were the most commonly used for external calibration purposes in previous *in situ* Ti-oxide studies conducted by LA-ICP-MS (e.g., Choukroun *et al.* 2005, Klemme *et al.* 2006, Charlier *et al.* 2007). These glasses have been nominally doped to $\sim$ 500 and $\sim$ 50 $\mu g\ g^{-1}$, respectively, for a broad range of trace elements (Pearce *et al.* 1997). However, some chemical characterisation studies have shown heterogeneous distribution for certain elements (Eggins and Shelley 2002). Recently, efforts have been made to synthesise new reference materials suitable for *in situ* ilmenite analysis; for example, Ødegård *et al.* (2005) produced a titanite ($CaTiSiO_5$) glass calibration material (TIT-200) doped to $\sim$ 200 $\mu g\ g^{-1}$ for a variety of elements of interest. The use of the TIT-200 glass by Charlier *et al.* (2007) exhibited its usefulness as a calibrator, as well as revealing one major drawback – the lack of certain elements of interest (e.g., Ta), thus requiring the use of other reference materials (NIST SRM 610) for their abundance determinations. Regardless, the TIT-200 glass is no longer available for distribution (S. Øyvind, Geological Survey of Norway, pers. comm.). Klemme *et al.* (2008) have recently created a new titanite glass that may be utilised in a manner similar to the TIT-200 glass, but lacks several elements of significance typically found in ilmenite (V, Co, Ni, Cu).

In an attempt to address the important issues of matrix matching, determination of appropriate elements and sufficient material for large-scale distribution in relation to ilmenite studies, we conducted a detailed chemical investigation of natural ilmenite megacrysts retrieved from stream deposits on the Island of Malaita, Solomon Islands. The ilmenite megacrysts are derived from proximal alnöite pipes (Neal 1986, Neal and Davidson 1989) that were emplaced between $\sim$ 52 and $\sim$ 35 Ma (Simonetti and Neal 2010). We had in our possession twenty-three ilmenite megacrysts that were $\sim$ 2–4 cm in diameter, then split into multiple fractions and subsequently analysed by electron probe microanalysis for their major element composition. Chemically digested fractions were subsequently analysed by solution-mode ICP-MS, and solid fragments were investigated *in situ* using laser ablation ICP-MS. We report on these comparative results and comment on the precision and accuracy of the analytical protocol developed, and potential use of the Malaitan ilmenite megacrysts as working reference materials.

Analytical methods

Seven of the largest ilmenite megacrysts exhibiting the least amount of surface alteration were chosen for analysis and designated sample names CRN63E to K. Samples were cut into thirds and further trimmed to remove surface alteration features. One-third was crushed and a fraction (0.42–0.59 mm) was separated by sieve for analysis by solution-mode ICP-MS. The latter fractions were cleaned in a 5% v/v HNO_3 ultrasonic bath for 25 min, handpicked for purity under a binocular microscope and ground to a powder in an agate mortar. The mortar and pestle were cleaned after each sample by rinsing in 18 MΩ water, 5% v/v nitric acid and acetone. Samples ($\sim$ 20–35 mg) were dissolved in $\sim$ 5 ml of 6 mol l^{-1} HCl in 15-ml Savillex® Teflon vials on a hotplate set at 200 °C for 7 d. Samples were then evaporated to dryness followed by the addition of 5 ml HCl (6 mol l^{-1}). The solutions were diluted to a final volume of $\sim$ 70 ml with 18 MΩ water.

Fourteen elements were quantified: Sc, Ti, V, Cr, Mn, Co, Ni, Cu, Zn, Zr, Nb, Sn, Hf and Ta; these were chosen for their importance in geochemical and petrological

studies. With the exception of vanadium, copper and zinc, the abundances of the remaining elements investigated by solution-mode ICP-MS were determined by a standard addition method (after Jenner *et al.* 1990). Vanadium was quantified in a separate run using three standard solutions (2, 25 and 100 ng g^{-1}) as calibrators. A 10 ng g^{-1}

Table 1.
Major and minor element compostion (% m/m) of Malaitan ilmenite megacrysts

Sample	CRN63E	CRN63F	CRN63G	CRN63H	CRN63I	CRN63J	CRN63K
TiO_2	50.2 (6)	51.7 (20)	51.8 (15)	50.6 (5)	51.8 (15)	52.0 (20)	51.1 (16)
Al_2O_3	0.43 (7)	0.51 (34)	0.58 (24)	0.69 (7)	0.57 (25)	0.44 (20)	0.41 (19)
FeO	41.8 (5)	38.4 (30)	38.2 (23)	41.2 (4)	37.7 (27)	38.8 (21)	40.9 (16)
MnO	0.31 (4)	0.28 (10)	0.27 (9)	0.21 (6)	0.33 (10)	0.24 (6)	0.26 (7)
MgO	6.1 (5)	7.9 (12)	8.3 (9)	6.49 (9)	8.5 (14)	7.97 (80)	6.27 (68)
V_2O_3	0.13 (5)	0.16 (6)	0.17 (6)	0.16 (5)	0.16 (6)	0.16 (7)	0.11 (4)
Total	99.05	98.93	99.29	99.3	99.02	99.65	99.05
n	6	16	13	11	10	8	9

n = number of analyses. Numbers in parentheses indicate the 2*s* value in terms of the last significant figures.

Table 2.
Major and minor element composition (% m/m) of the megacryst exsolution phase

Sample	CRN63E	CRN63F	CRN63G	CRN63I	CRN63J	CRN63K
TiO_2	21.9 (3)	21.6 (10)	21.0 (10)	21.5 (11)	21.1 (14)	20.9 (23)
Al_2O_3	4.13 (7)	5.7 (17)	7.5 (12)	6.5 (12)	7.1 (11)	4.9 (18)
FeO	66.2 (7)	62.7 (9)	61.3 (19)	61.5 (15)	62.8 (6)	66.5 (7)
MnO	0.31 (1)	0.28 (8)	0.28 (8)	0.34 (13)	0.27 (3)	0.27 (10)
MgO	4.6 (1)	6.4 (6)	7.1 (7)	7.2 (11)	6.3 (3)	4.9 (6)
V_2O_3	0.40 (5)	0.63 (5)	0.59 (7)	0.58 (4)	0.59 (5)	0.46 (4)
Total	97.47	97.24	97.85	97.53	98.17	97.95
n	3	6	5	4	3	3

n = number of analyses. Numbers in parentheses indicate the 2*s* value in terms of the last significant figures.

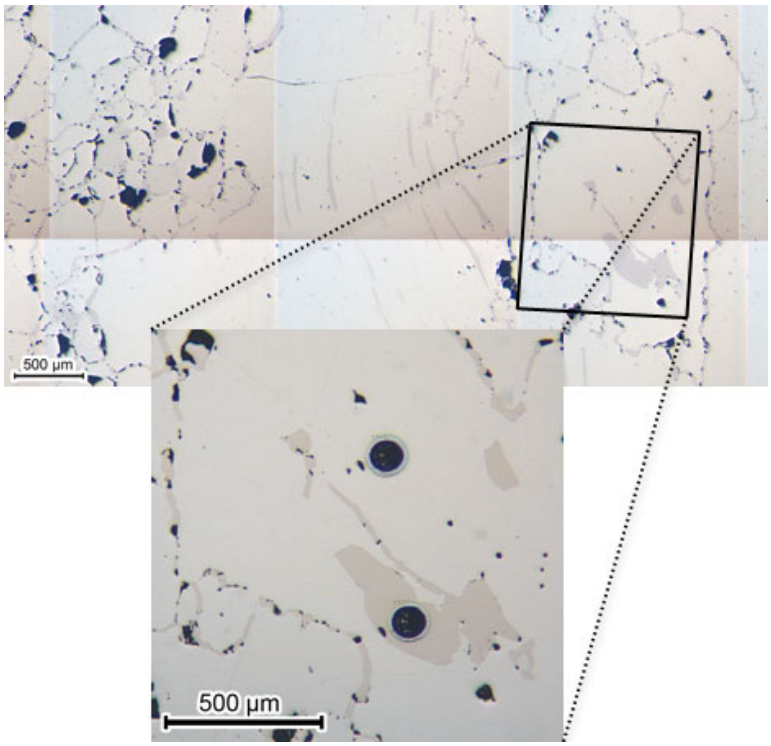

Figure 1. Reflected light portion of photomosaic (5 × magnification) of CRN63F showing the main textures exhibited by exsolution, as 'grain' boundaries and lamellae. Expanded image shows two 80 µm ablation pits.

vanadium solution introduced at a rate of ~ 0.5 ml min^{-1} yielded ~ 270000 cps in medium mass resolution analysis on the University of Notre Dame Element2 sector field high resolution (HR)-ICP-MS. Copper and zinc were quantified by external calibration using a four-point calibration curve (1, 20, 50, 100), where a 10 ng g^{-1} copper and zinc solution measured in medium resolution mode yielded ~ 200000 cps and ~ 70000 cps, respectively.

The portions of ilmenite megacrysts used for electron probe and laser ablation analyses were cut into ~ 3 mm-thick tabs and mounted on 1 inch epoxy rounds and polished. Major and minor element concentrations (Table 1) were determined on a JEOL JXA-8200 electron microprobe at Washington University, St. Louis. Analyses were acquired using the Probe for Windows software, and X-ray correction was performed using the CITZAF correction software (Armb 1995). A 5 to 10 μm beam size was used with a 20 kV accelerating potential and a 25 nA probe current. EPMA confirmed the presence of a Fe-Ti-rich exsolution phase (Table 2, Figure 1) in all samples, originally identified by reflected light microscopy.

In situ LA-ICP-MS analyses of ilmenite megacrysts to determine trace elements were performed on a Thermo Finnigan Element2 HR-ICP-MS (Thermo Fisher Scientific, Bremen, Germany) coupled to a NewWave Research UP213 Nd:YAG laser ablation system (ESI, Portland, OR, USA). Details of the instrument conditions and settings and analytical method employed are listed in Table 3. Prior to laser ablation analysis, optimisation of the ICP-MS instrument was achieved with the use of a 1 ng g^{-1} multi-element (mass range from Li to U) tuning solution (Table 3). Tuning consisted of optimisation of the torch assembly position, sample gas (Ar) flow rate, ion lens stack voltages and reference mass calibration. Subsequent to tuning and optimisation in solution mode, the instrument was shut down in order to change the introduction system to laser ablation mode. The optimum carrier gas (He) flow rate into the laser ablation cell was determined by running the laser in scanning mode over a NIST SRM 610 glass bead in order to obtain maximum ion signal intensities and minimum oxide levels (typically ‹ 3% as monitored by the Th/ThO ratio in both solution and laser ablation modes); this was typically achieved at a flow rate of ~ 0.7 l min^{-1}. The NIST SRM 610 glass bead was placed adjacent to the round 1 inch in diameter glass slide holding the ilmenite megacrysts samples within the standard laser ablation cell. This facilitated the use of NIST SRM 610 as calibrator, avoiding disruption to the plasma as this set-up eliminated the additional step of having to open the laser ablation cell in order to exchange mounts/samples. After sample exchange, 15–20 min were allowed to elapse prior to the resumption of lasering in order to ensure re-equilibration between the laser ablation cell and the ICP-MS introduction system. A typical sample analysis consisted of ~ 60 s of background measurement followed by ablation and ion signal acquisition for ~ 60 s. Ablated particles were transported to the ICP-MS torch via the sample outline (0.25 inch outer diameter St. Gobain Tygon tubing) that was 'Y'-connected to the Ar gas sample outline prior to the torch. All laser ablation analyses were conducted in medium mass resolution (resolution = mass/peak width ~ 4000) in order to eliminate any potential spectral interferences. The reduction in sensitivity (roughly one order of magnitude) that is experienced for analyses conducted at medium mass resolution (relative to low resolution) permitted the use of ^{46}Ti as the

Table 3.
LA-ICP-MS operating conditions and data acquisition parameters

ICP-MS	
Type	Magnetic Sectorfield
Brand and model	ThermoFinnigan Element2
Forward power	1250 W
Cooling gas (Ar)	16.1 l min^{-1}
Auxiliary gas (Ar)	0.94 l min^{-1}
Sample gas (Ar)	1.123 l min^{-1}
Carrier gas (He)	0.7 l min^{-1}
LASER	
Type	Nd:YAG
Brand and model	New Wave Research UP213
Wavelength	213 nm
Pulse duration	5 ns
Spot size	80 μm
Repetition rate	5 Hz
Nominal energy output	100%
Laser fluency	20.3–22.14 J cm^{-2}
Data acquisition parameters	
Resolution mode	Medium
Data acquisition protocol	Time-resolved analysis
Scan mode	E-scan
Scanned masses	^{45}Sc, ^{46}Ti, ^{51}V, ^{53}Cr, ^{55}Mn, ^{59}Co, ^{60}Ni, ^{63}Cu, ^{68}Zn, ^{90}Zr, ^{93}Nb, ^{120}Sn, ^{180}Hf, ^{181}Ta
Settling time	0.001–0.300 s
Sample time	0.01 s
Samples per peak	20
Number of scans	23 (23 runs × 1 pass)
Detector mode	Both
Detector deadtime	13 ns
Background collection	60 s
Ablation time for age calculation	60 s
Washout	30 s
Standardisation and data reduction	
External calibrator	NIST SRM 610
Data reduction software used	GLITTER©

Table 4.
Trace element composition (μg g^{-1}) of Malaitan ilmenite megacrysts

Sample	Sc	V	Cr	Mn	Co	Ni	Cu	Zn	Zr	Nb	Sn	Hf	Ta
DL-S	0.04	2.22	0.02	N.A.	0.001	0.24	0.16	0.99	0.02	0.01	0.09	0.01	0.001
63E-S	11.6	1086	1.00	N.A.	202	238	11.3	209	213	362	7.55	12	40.3
63E-LA	9.8 (1.1)	1062 (106)	‹ 1.25	2601 (302)	161 (7)	27.8 (15)	7.13 (1.60)	292 (17)	254 (34)	299 (23)	5.85 (0.14)	8.09 (1.41)	29.2 (3.0)
63E-2σ	2.8	224		583	15	12.3	2.08	75	61	64	1.73	2.18	5.3
63F-S	11.5	1297	3.63	N.A.	174	215	12.7	178	144	141	5.37	4.99	1.98
63F-LA	16.0 (4.0)	1546 (429)	3.79 (1.60)	2588 (1087)	207 (13)	222 (50)	7.50 (4.31)	226 (44)	248 (73)	185 (18)	5.06 (1.11)	7.54 (1.46)	19.7 (3.1)
63F-2σ	3.1	136	3.19	459	32	32	1.83	23	47	26	1.49	2.36	2.3
63G-S	11.8	1285	7.81	N.A.	233	295	11.7	183	114	96.7	4.43	4.28	0.56
63G-LA	12.1 (2.6)	1369 (373)	6.70 (5.18)	2219 (849)	203 (40)	283 (133)	11.1 (7.4)	252 (161)	152 (31)	122 (5)	3.93 (0.50)	4.77 (0.70)	10.6 (1.1)
63G-2σ	2.8	217	3.49	256	18	32	3.1	25	34	16	1.29	1.41	2.7
63H-S	9.18	1216	‹ b.d.	N.A.	161	85	9.28	242	105	132	4.25	5.18	12.5
63H-LA	11.6 (1.7)	1272 (115)	‹ 1.4	1800 (259)	195 (5)	97.8 (13)	10.0 (2.0)	288 (30)	155 (19)	144 (17)	4.30 (0.69)	5.16 (0.77)	13.6 (5.2)
63H-2σ	4.2	237		565	35	28.7	4.1	44	37	14	1.32	1.55	4.1
63I-S	74.1	1393	N.A.	N.A.	1136	2234	9.39	206	115	153	7.9	9.68	68.2
63I-LA	13.2 (1.7)	1422 (268)	3.43 (0.80)	2649 (587)	203 (22)	268 (70)	6.97 (6.12)	218 (52)	183 (36)	159 (11)	4.88 (1.00)	5.76 (1.02)	16.0 (1.4)
63I-2σ	7.5	374	2.61	971	36	143	2.58	71	66	20	2.18	1.83	4.3
63J-S	7.15	1265	N.A.	N.A.	147	272	18.4	201	105	95.2	4.52	5.26	4.78
63J-LA	12.4 (2.0)	1294 (345)	5.23 (1.26)	2026 (423)	200 (27)	264 (64)	3.96 (7.98)	204 (43)	162 (20)	141 (8)	4.12 (1.15)	5.40 (0.73)	13.7 (1.0)
63J-2σ	2.5	231	3.79	311	25	55	1.33	63	26	18	1.47	1.71	1.9
63K-S	‹ b.d.	1071	1.69	N.A.	‹ b.d.	‹ b.d.	6.45	200	141	170	5.34	5.81	48.2
63K-LA	11.1 (2.2)	1136 (262)	1.04	2294 (243)	193 (13)	58.2 (11)	1.50 (1.19)	284 (50)	212 (33)	221 (9)	4.81 (1.22)	7.03 (1.07)	24.0 (2.0)
63K-2σ	2.3	303	1.46	392	58	19.0	1.07	54	49	78	1.44	2.23	6.0
Exsolution phase													
63E-LA	2.28	2169	2.47	2095	249	43.3	38.1	1062	36.9	102	5.16	1.71	13.5
63F-LA	5.63	1188	6.98	1494	140	178	7.95	250	82.1	79	2.69	2.67	9.29
63G-LA	4.99	2147	18.8	1285	181	325	24.8	466	45.3	41.6	2.72	1.57	4.79
63I-LA	4.8	1117	5.35	1904	121	295	9.83	239	52.1	80	2.18	1.99	8.78
63J-LA	4.23	436	1.85	951	89.1	119	‹ 0.42	82.6	52.9	69.6	1.6	1.95	6.7
63K-LA	3.61	3200	4.57	2939	320	185	45.3	1187	38.6	28.9	5.49	1.68	3.99

DL-S, detection limit in solution mode; S, solution mode; LA, laser ablation mode with standard deviation (2*s* level) in parenthesis; 2σ, average Glitter estimated uncertainty (2*s* level); ‹ b.d., below detection limit; N.A., not analysed.

GEOSTANDARDS and GEOANALYTICAL RESEARCH

GEOSTANDARDS and GEOANALYTICAL RESEARCH

Table 5.
Trace element values (μg g^{-1}) for NIST SRM 610 and MPI-DING reference materials obtained by LA-ICP-MS

Element	DL	Isotope (amu)	NIST SRM 610			MPI-DING ML3B-G				MPI-DING KL2-G			
			This study			This study		Jochum *et al.* (2006)		This study		Jochum *et al.* (2006)	
			Average	SD (2*s*)	Accepted	Average	SD (2*s*)	Preferred value	Range	Average	SD (2*s*)	Preferred value	Range
			LA-ICP-MS			LA-ICP-MS (n = 10)				LA-ICP-MS (n = 7)			
Sc	0.18	45	449	37	441	26.3	5.8	31.6	1.6	31.2	5.8	31.8	0.9
V	0.60	51	446	24	442	310	24	268	23	366	47	309	38
Cr	1.06	53	408	27	405	169	9	177	23	326	53	294	27
Mn	0.40	55	438	29	433	1476	100	1316	70	1396	45	1277	70
Co	0.24	59	407	18	405	48.7	4.5	41.2	3.5	51.3	9	41.2	2.3
Ni	7.45	60	450	35	444	118	7	107	9	119	9	112	5
Cu	0.69	63	435	28	430	130	6	112	10	99	5	87.9	9.1
Zn	0.93	68	460	25	456	132	4	108	14	125	6	110	10
Zr	0.50	90	445	30	440	105	26	122	3	152	42	152	5
Nb	0.07	93	423	22	419	8.32	0.27	8.6	0.22	15.9	1.2	15	0.5
Sn	0.32	120	402	28	396	1.74	0.19	1.14	0.33	2.50	1.4	1.54	0.29
Hf	0.11	180	419	16	418	2.64	0.68	3.22	0.08	3.96	1.2	3.93	0.14
Ta	0.05	181	380	20	377	0.43	0.05	0.555	0.013	0.98	0.33	0.961	0.022

Average NIST SRM 610 values from twenty-eight analyses. DL, detection limit; amu, atomic mass unit; SD, standard deviation (2*s*). Values for NIST SRM 610 from Pearce *et al.* (1997).

internal standard for all analyses, despite its ~ 50% m/m TiO_2 abundance in ilmenite (determined by EPMA). The analysis of every ten unknowns was bracketed by the repeated analysis of the NIST SRM 610 glass (n = 4; two prior and two subsequent analyses of unknowns) for external calibration purposes. For each ilmenite sample, a minimum of five laser ablation analyses were conducted over the entire section (Table 4, Figure 1). Detailed photomicrographs taken prior to ilmenite analysis allowed the exsolution phase to be avoided during the laser ablation experiments. Accidental sampling of the exsolution phase would have been apparent in the Glitter time-resolved spectra in relation to the ^{46}Ti ion signal intensity (i.e., TiO_2 content was less than half compared with ilmenite, Tables 1 and 2). With the exception of sample CRN63H, at least one laser ablation analysis of the exsolution phase from each sample was performed when possible (i.e., given the 80 μm spot size – Table 3). Laser ablation experiments for the quantification of trace element abundances were conducted over the same areas analysed for major elements by EPMA, thus ensuring that the concentration of the internal standard ^{46}Ti was accurately known for each laser ablation analysis. Concentration determinations, associated uncertainties (2*s*) and detection limits obtained by LA-ICP-MS for the ilmenite megacrysts investigated here are listed in Table 4.

The accuracy of our laser ablation method was also verified by the analysis of two MPI-DING (Max Planck Institut–Dingwell, Mainz, Germany; Jochum *et al.* 2006) synthetic silicate glasses KL2-G (Kilauea tholeiitic basalt glass) and ML3B-G (Mauna Loa tholeiitic basalt glass); both contain similar abundance levels for the trace elements in the ilmenites investigated here. The internal standard employed was ^{46}Ti. Calculated average abundances obtained from repeated analyses (n = 7 and 10, respectively) of the glasses corresponded well with accepted values, with few exceptions (Table 5). Copper, Zn and Ta abundances obtained for ML3B-G were 2–5% higher than the range of the reported reference values. The abundance of Sn was underestimated (12%); however, compared with the majority of the remaining elements investigated (Jochum *et al.* 2006), the abundance of Sn in RM ML3B-G is extremely low at 1.54 μg g^{-1} (Table 5). Alternatively, the lack of correspondence for these elements may be in part due to a heterogeneous distribution of certain chalcophile elements as noted by Jochum *et al.* (2006). MnO (% m/m) in KL2-G was also slightly overestimated compared with the preferred values but was within the full range of abundances measured in the glass (Jochum *et al.* 2006). The standard deviation (2*s*) and detection limits (μg g^{-1}) associated with the elements investigated here and for the two MPI-DING reference glasses are listed in Tables 4 and 5.

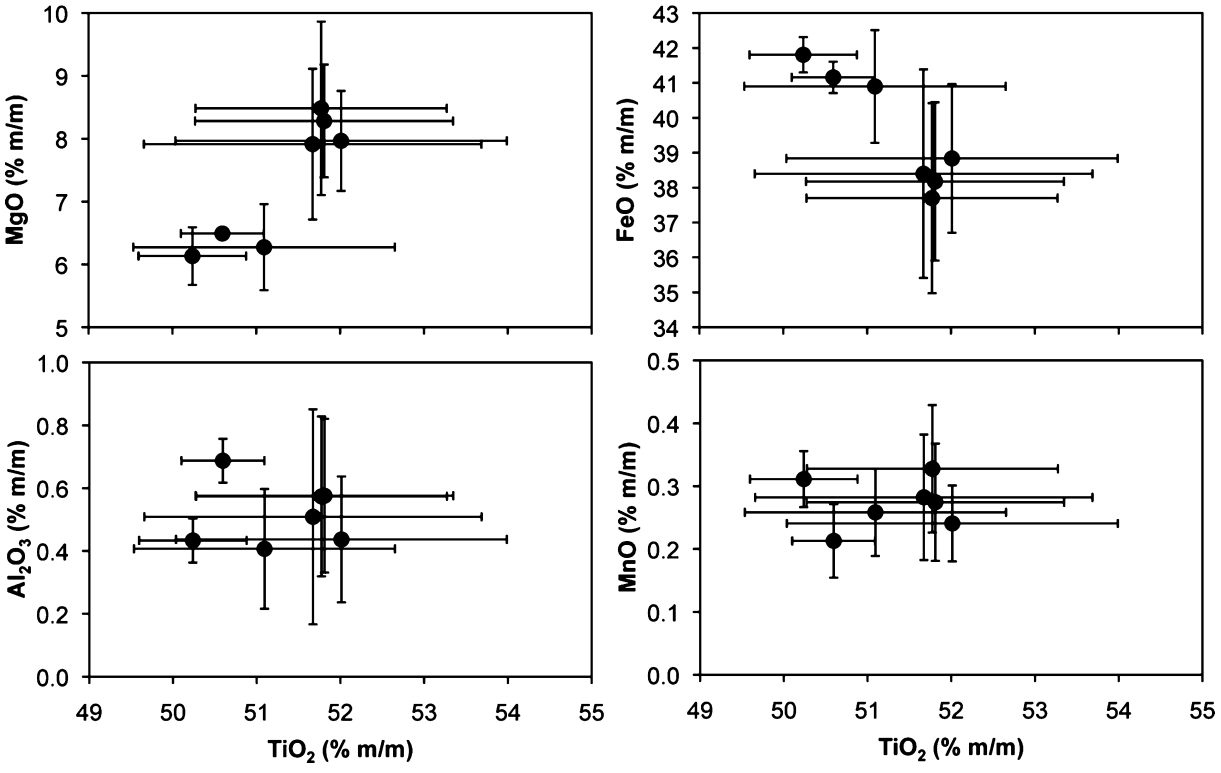

Figure 2. Average major element content in ilmenite (% m/m). Error bars are at the 2*s* level (from Table 1).

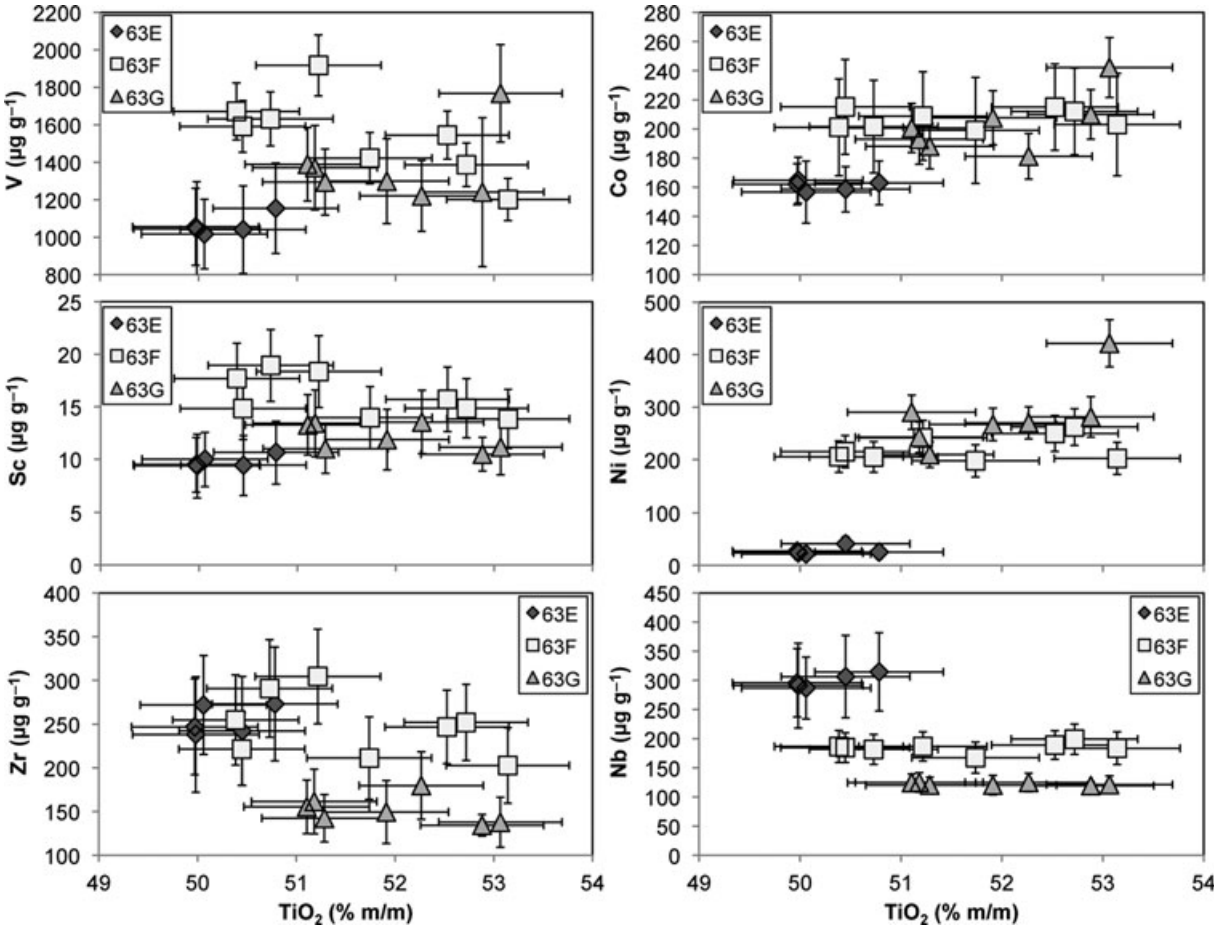

Figure 3. Trace element values (µg g^{-1}) plotted against average TiO_2 (% m/m) content.

Results and discussion

Major element concentrations (Table 1) between the ilmenite megacrysts overlapped for TiO_2 (49.72–53.77% m/m) and MnO (0.15–0.40% m/m); TiO_2 and MgO (5.77–9.42% m/m) contents were positively correlated, whereas TiO_2 correlated negatively with FeO (35.75–42.27% m/m) abundances and indicated no trend with Al_2O_3 (0.22–0.77% m/m) concentrations (Figure 2). These trends are consistent with progressive crystallisation from an evolving magma (Nixon and Boyd 1979, Neal and Davidson 1989). The exsolution phase composition (Table 2) appears to be of titano-magnetite spinel composition identified previously by Neal and Davidson (1989). Based on the variation in major element abundances (Figure 2), it is clear that the Malaitan ilmenite megacrysts are not entirely homogeneous. Thus, if fragments are indeed eventually distributed to interested laboratories, each fragment would require analysis by electron microprobe to characterise the major element abundances.

With regard to trace element abundances (Table 4), our preliminary characterisation indicated chemical heterogeneity at the < 100 µm scale within individual samples. Sample CRN63E exhibited the least amount of exsolution features and appeared to be the most homogeneous sample. For sample CRN63E, the calculated analytical uncertainties (i.e., precision at the 2*s* level) associated with individual determinations for all elements except Ni as determined by GLITTER were slightly larger (varying between 10% and 30%) compared with the relative standard deviation (% RSD varying between 2% and 22% at the 2*s* level; Table 4). Moreover, Sc, V, Mn, Co, Zn, Zr, Sn and Hf abundances appeared to be homogeneous for samples CRN63E, H and K because their associated % RSD values were < 20% (2*s* level) in general.

The ilmenite megacrysts investigated here were collected from stream deposits, thus rendering any attempt at unravelling their petrogenetic relationship somewhat difficult. Variable element concentrations may be due to spatial (i.e., magma heterogeneity) or temporal (i.e., magma

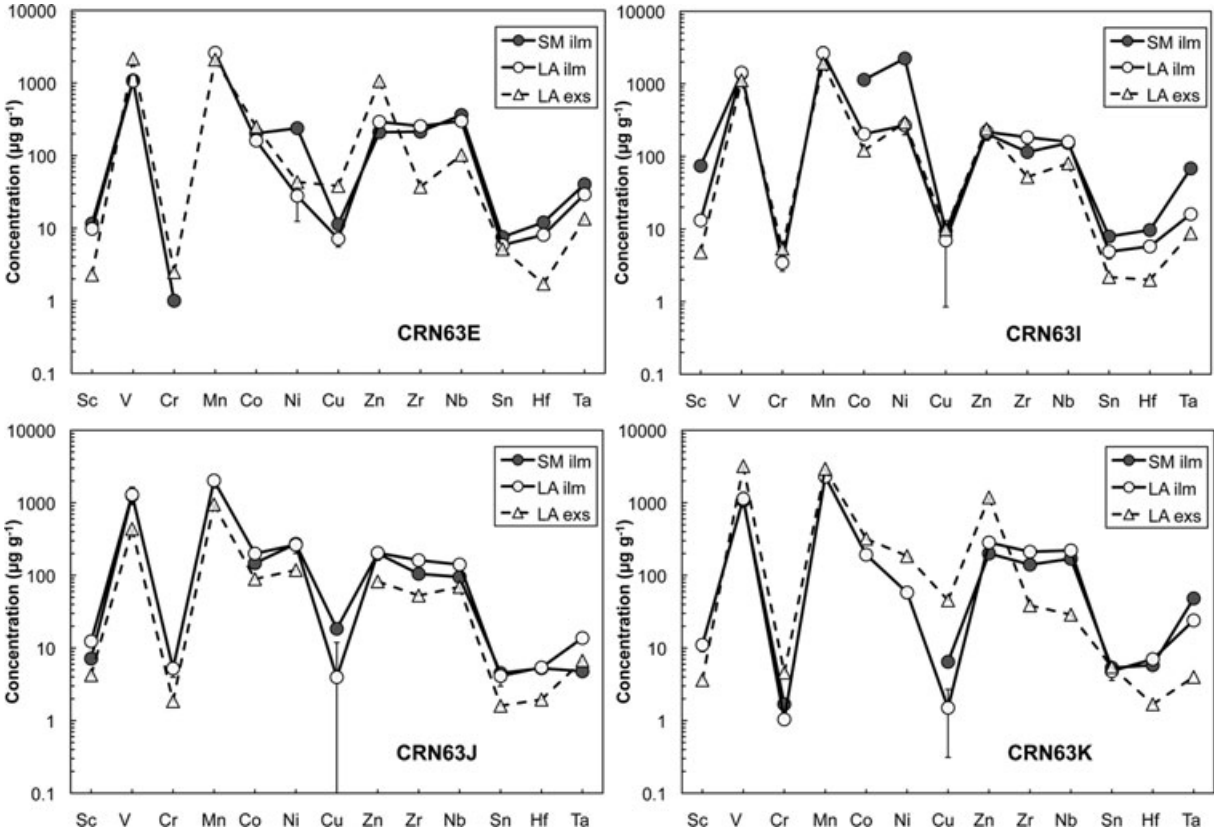

Figure 4. Comparison of trace element values obtained by laser ablation and solution-mode ICP-MS for ilmenite and exsolution phases of samples CRN63E, I, J and K. Error bars (2*s*) shown for LA-ICP-MS only (from Table 4).

evolution) differences. However, TiO_2 and MgO contents (Figure 2) can be utilised to group the ilmenite into primitive (CRN63F, G, I, J; high MgO of 7.9–8.5% m/m) and more evolved (CRN63E, H, K; low MgO of 6.1–6.5% m/m) samples. In general, trace element abundances were similar between samples, although Ni (283–27 µg g^{-1}) was lower in samples with lesser MgO contents. Despite some major element variability within individual ilmenite megacryst samples, there was no apparent correlation between major and trace element abundances (Figure 3), in particular for the most homogeneous sample (CRN63E) and two relatively heterogeneous samples (CRN63F, G). The relatively small proportion of ilmenite megacrysts present in the alnöite melt (0.5%; Neal and Davidson 1989) may have been insufficient to significantly fractionate the host magma, resulting in the lack of correlation for elements incorporated into ilmenite (Mitchell 1977).

A comparison between solution-mode and laser ablation ICP-MS results indicated good agreement for the majority of the elements investigated here. Figures 4 and 5 illustrate a comparison between averages for laser ablation analyses of the ilmenites and contained exsolution phase as well as solution-mode runs. The exsolution phase was found to be relatively depleted in incompatible elements Zr, Nb, Hf and Ta, but otherwise similar to the ilmenite phase. Dissolution of the exsolution phase during acid digestion may be responsible for a significant number of solution-mode analyses with values that are intermediate between those obtained for ilmenite and exsolution phase during laser ablation runs (e.g., CRN63J and K in Figure 4). However, not all of the variation can be explained by exsolution phase 'contamination'. Figure 6, a series of log–log plots, illustrates that the elemental abundances obtained via LA-ICP-MS were within an order of magnitude between samples, whereas those for several elements measured via solution-mode analysis varied over several orders of magnitude (e.g., Figure 6d, g, i). In general, samples with disparate LA- and solution-ICP-MS values had more variable solution-ICP-MS values, indicating issues with ilmenite dissolution. This interpretation is corroborated by the fact there was good agreement between the results for repeat LA-ICP-MS analyses of NIST SRM 610 and MPI-DING reference materials relative to their reference values.

Solution-mode analysis monitored ^{65}Cu and ^{66}Zn and yielded inconsistent and highly variable results for samples

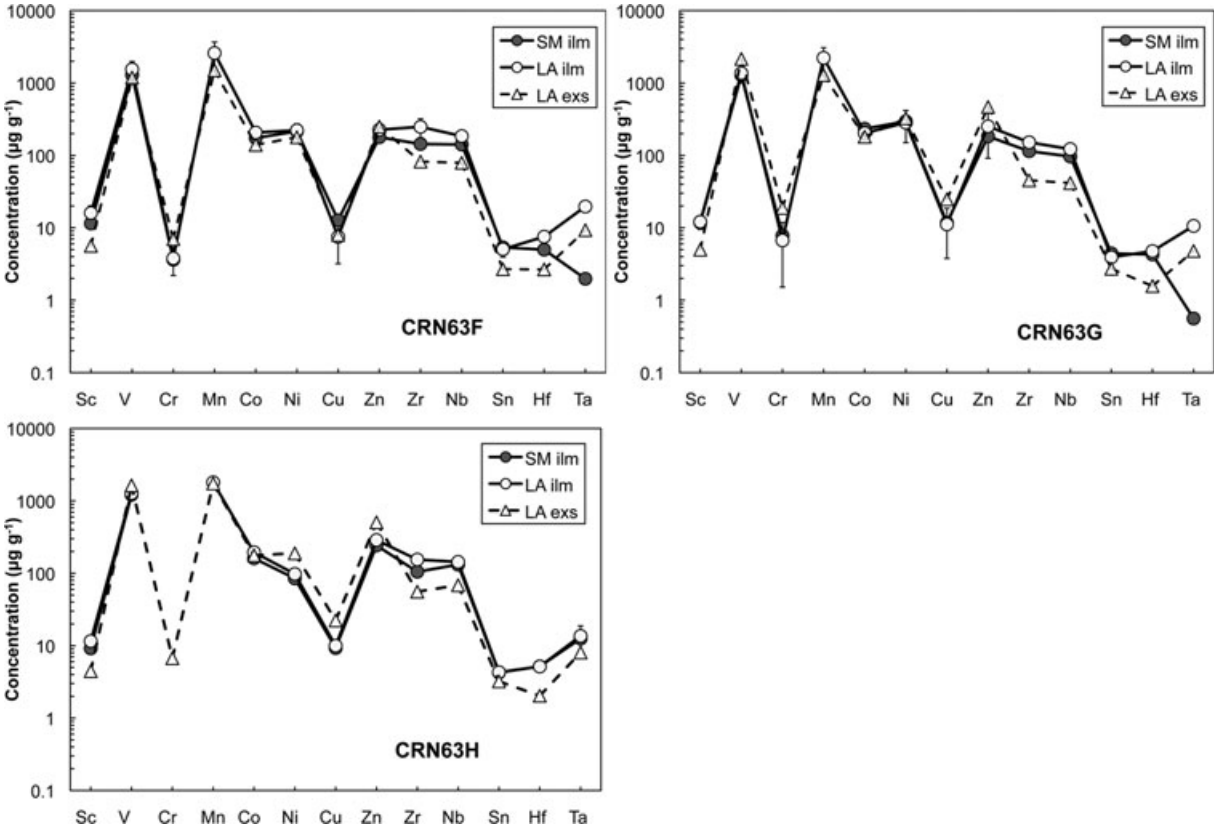

Figure 5. Comparison of trace element values obtained by laser ablation and solution-mode ICP-MS for ilmenite and exsolution phases of samples CRN63F, G and H. Error bars (2*s*) shown for LA-ICP-MS only (from Table 4). For sample 63H, displayed average exsolution values are the averages of all samples.

from the same parental solution. Concentrations obtained via laser ablation monitored ^{63}Cu and ^{68}Zn and yielded more consistent results (Table 4). Thus, additional solution-mode analyses of the same solutions were conducted by spike addition, which monitored multiple isotopes of the same element (^{63}Cu, ^{65}Cu, ^{66}Zn, ^{68}Zn, ^{90}Zr, ^{92}Zr and ^{93}Nb) to assess the possibility of spectral interferences (Table 6). The results listed in Table 6 indicate that Zr concentrations did not vary significantly from each other and that Zr and Nb abundances were similar to those obtained by laser ablation. However, calculated abundances based on the ^{65}Cu and ^{66}Zn ion signal measurements were 2–3 and 4–8 times higher, respectively, than for concentrations determined using the ^{63}Cu and ^{68}Zn signal intensities. In addition, the calculated abundances of Cu and Zn based on the latter were in good agreement with those obtained via LA-ICP-MS (Tables 4 and 5). For an ilmenite-based matrix, important spectroscopic interferences at masses 65 and 66 possibly include ^{48}Ti^{16}O^{1}H^{+}, ^{49}Ti^{16}O^{1}H^{+} and ^{40}Ar^{26}Mg, which may explain the elevated signals (and corresponding elevated calculated abundances).

To assess the benefits of utilising a matrix-matched, ilmenite reference material as opposed to the NIST SRM 610 glass in LA-ICP-MS analysis, individual analyses of CRN63E (the most homogeneous sample) were reprocessed using the average, laser ablation-based composition of CRN63E (Table 4). Data were reprocessed using the GLITTER software (GEMOC, Macquarie University, Australia) by creating an external calibrator (.txt) file and equating it to analysis #2 (the most precise run). Table 7 lists the concentrations determined for the same elements using the two different reference samples (NIST SRM 610 *vs.* CRN63E-2), and these indicated similar comparative results. Assuming that utilising a matrix-matched, ilmenite reference sample is the best approach, then the external calibration using the NIST SRM 610 glass will always underestimate, on average, the Mn and Ni abundances by 9% and 26%, respectively. Average deviations for the remaining elements were within ± 6% and therefore well within the level of the associated % RSD for most elements investigated here. Thus, it would seem that Mn and Ni abundances may be suspect when using the NIST SRM 610 glass as the external calibrator; the accuracy of an

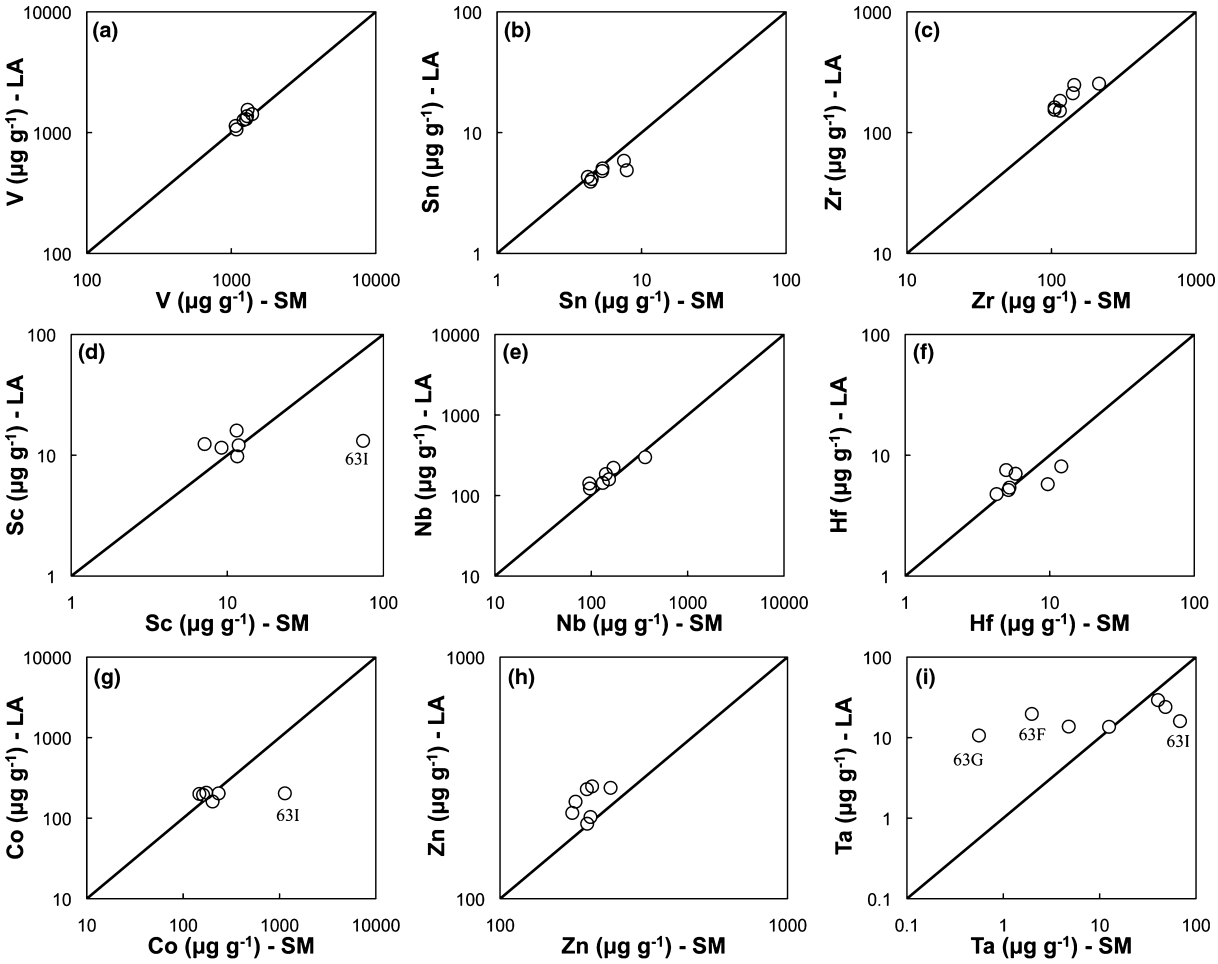

Figure 6. Comparison of trace element abundances determined by laser ablation (LA) and solution-mode (SM) ICP-MS for selected elements from Table 4. A 1:1 ratio line is drawn in each plot for comparison purposes. Note: Sc and Co abundances for 63K-S were below detection limit and are therefore not plotted.

Table 6.
Elemental abundances (µg g^{-1}) for ilmenite megacrysts obtained by solution-mode ICP-MS

Isotope	Cu		Zn		Zr		Nb
	^{63}Cu	^{65}Cu	^{66}Zn	^{68}Zn	^{90}Zr	^{92}Zr	^{93}Nb
CRN63E	11.3	84.5	516	209	202	210	280
CRN63F	12.7	83.8	482	178	151	155	133
CRN63G	11.7	72.7	463	183	117	122	80.4
CRN63H	9.28	72.2	477	242	107	109	139
CRN63I	9.39	68.3	447	206	115	120	153
CRN63J	18.4	72.3	447	201	105	107	95.2
CRN63K	6.45	62.2	430	200	141	143	170

ilmenite-based external calibrator approach will be investigated in future studies.

Advances in LA-ICP-MS technology and instrumentation that have occurred during the past decade must be accompanied by the availability of matrix-matched reference materials, in particular those for non-silicate minerals. Despite the few shortcomings of this sample set in relation to major and trace element variations, laboratories wishing to analyse ilmenite may, nonetheless, find them useful for reference purposes. Alternatively, these ilmenite megacrysts may serve as versatile internal laboratory reference samples

Table 7.
Comparison of CRN63E trace element abundances (μg g^{-1}) standardised to NIST SRM 610 and average CRN63E values

Element	63E-1 (exsolution)		63E-2		63E-3		63E-4		63E-5		63E-6	
	SRM 610	63E ilm.	SRM 610	63E ilm.	SRM 610	63E ilm.	SRM 610	63E ilm.	SRM 610	63E ilm.	SRM 610	63E ilm.
Sc	2.28	2.23	10	9.79	9.5	9.26	10.7	10.4	9.43	9.16	9.38	9.11
V	2169	2234	1017	1062	1056	1110	1154	1226	1041	1116	1044	1131
Mn	2095	2315	2354	2601	2668	2924	2565	2800	2692	2926	2729	2954
Co	249	254	157	161	162	166	163	168	159	164	165	171
Ni	43.3	55.3	21.8	27.8	27.3	34.7	25.4	32.0	41.1	51.8	23.6	29.6
Cu	38.1	38	7.1	7.13	7.57	7.6	6.16	6.2	6.61	6.68	8.21	8.32
Zn	1062	1061	286	292	304	315	290	306	295	316	283	308
Zr	36.9	34.2	272	254	247	231	273	257	242	229	238	226
Nb	102	106	287	299	296	307	315	326	306	318	291	302
Sn	5.16	5.06	5.87	5.85	5.86	5.88	5.81	5.89	5.94	6.09	5.75	5.96
Hf	1.71	1.62	8.51	8.09	8.03	7.61	9.01	8.54	7.69	7.29	7.2	6.83
Ta	13.5	13.0	29.9	29.2	28.5	27.9	31.5	30.9	28.7	28.3	27.6	27.4

with the elemental abundances obtained by LA-ICP-MS (Table 4) utilised as working values for individual megacrysts. We estimate that our ilmenite megacryst sample collection can make available a minimum of 60 (millimetre-sized) fragments for distribution to interested laboratories.

Conclusions

The investigation described here indicates that the CRN63 ilmenite megacrysts are not suitable for consideration as a *certified* reference material. However, as with previous investigations of a similar nature, we do confirm that accurate element abundances in ilmenite may be obtained at high spatial resolution via the use of titanium as the internal standard and the NIST SRM 610 glass for external calibration. Hence, we do have available ilmenite megacryst fragments for distribution to interested laboratories. As demonstrated here, however, additional ilmenite fragments would require major element characterisation prior to their use as internal laboratory reference materials. Finally, this study also contributes an additional data set of elemental abundances for the two MPI-DING reference glasses ML3B-G and KL2-G.

Acknowledgements

We thank Sandy Dillard (Brazos Valley Petrographic and Thin Section Service) for preparation of polished ilmenite mounts. Paul Carpenter (Washington University, St. Louis) is thanked for assistance with microprobe analyses. We thank K.P. Jochum (Max-Planck-Institut fur Chemie, Mainz) for supplying MPI-DING glasses. C.R. Neal also acknowledges the dedicated people at the Solomon Islands Geological Survey in Honiara for their support of field studies on Malaita and the people of central North Malaita for their generous hospitality. Comments from three anonymous reviewers helped in improving the quality of the manuscript. This study was supported in part by National Aeronautics and Space Administration grant NNX09AB92G to C.R. Neal.

References

Armb J.T. (1995)
CITZAF: A package of correction programs for the quantitative electron microbeam X-ray analysis of thick polished materials, thin films, and particles. **Microbeam Analysis, 4,** 177–200.

Brown G.M., Peckett A., Emeleus C.H., Phillips R. and Pinsent R.H. (1975)
Petrology and mineralogy of Apollo 17 mare basalts. Proceedings from the 6th Lunar Science Conference, 1–13.

Charlier B., Skår Ø., Korneliussen A., Duchesne J.C. and Auwera J.V. (2007)
Ilmenite composition in the Tellnes Fe-Ti deposit, SW Norway: Fractional crystallization, postcumulus evolution and ilmenite-zircon relation. **Contributions to Mineralogy and Petrology, 154,** 119–134.

Choukroun M., O'Reilly S.Y., Griffin W.L., Pearson N.J. and Dawson J.B. (2005)
Hf isotopes of MARID (mica-amphibole-rutile-ilmenite-diopside) rutile trace metasomatic processes in the lithospheric mantle. **Geology, 33,** 45–48.

Dymek R.F., Albee A.L. and Chodos A.A. (1975)
Comparative mineralogy and petrology of Apollo 17 mare basalts: Samples 70215, 71055, 74255, and 75055. Proceedings from the 6th Lunar Science Conference, 49–77.

Eggins S.M. and Shelley J.M.G. (2002)
Compositional heterogeneity in NIST SRM 610-617 glasses. **Geostandards Newsletter: The Journal of Geostandards and Geoanalysis, 26,** 269–286.

references

El Goresy A., Ramdohr P. and Taylor L.A. (1971)
The geochemistry of the opaque minerals in Apollo 14 crystalline rocks. Earth and Planetary Science Letters, 13, 121–129.

Jenner G.A., Longerich H.P., Jackson S.E. and Fryer B.J. (1990)
ICP-MS – A powerful tool for high-precision trace-element analysis in Earth Sciences: Evidence from analysis of selected U.S.G.S. reference samples. Chemical Geology, 83, 133–148.

Jochum K.P., Stoll B., Herwig K., Willbold M., Hofmann A.W., Amini M., Aarburg S., Abouchami W., Hellebrand E., Mocek B., Raczek I., Stracke A., Alard O., Bouman C., Becker S., Dücking M., Brätz H., Klemd R., de Bruin D., Canil D., Cornell D., de Hoog C.J., Dalpé C., Danyushevsky L., Eisenhauer A., Gao Y., Snow J.E., Groschopf N., Günther D., Latkoczy C., Guillong M., Hauri E.H., Höfer H.E., Lahaye Y., Horz K., Jacob D.E., Kasemann S.A., Kent A.J.R., Ludwig T., Zack T., Mason P.R.D., Meixner A., Rosner M., Misawa K., Nash B.P., Pfänder J., Premo W.R., Sun W.D.D., Tiepolo M., Vannucci R., Vennemann T., Wayne D. and Woodhead J.D. (2006)
MPI-DING reference glasses for *in-situ* microanalysis: New reference values for element concentrations and isotope ratios. Geochemistry Geophysics Geosystems, 7, 1–44.

Klemme S., Günther D., Hametner K., Prowatke S. and Zack T. (2006)
The partitioning of trace elements between ilmenite, ulvospinel, armalcolite and silicate melts with implications for the early differentiation of the moon. Chemical Geology, 234, 251–263.

Klemme S., Prowatke S., Münker C., Magee C.W., Lahaye Y., Zack T., Kasemann S.A., Cabato E.J.A. and Kaeser B. (2008)
Synthesis and preliminary characterisation of new silicate, phosphate and titanite reference glasses. Geostandards and Geoanalytical Research, 32, 39–54.

McCallum I.S. and Charette M.P. (1978)
Zr and Nb partition coefficients: Implications for the genesis of mare basalts, KREEP, and sea floor basalts. Geochimica et Cosmochimica Acta, 42, 859–869.

McKay G.A., Wagstaff J. and Yang S.-R. (1986)
Zirconium, hafnium and rare Earth element partition coefficients for ilmenite and other minerals in high-Ti lunar mare basalts. Journal of Geophysical Research, 91, 229–237.

Mitchell R.H. (1977)
Geochemistry of magnesian ilmenites from kimberlites from South Africa and Lesotho. Lithos, 10, 29–37.

Moore R.O., Griffin W.L., Gurney J.J., Ryan C.G., Cousens D.R., Sie S.H. and Suter G.F. (1992)
Trace element geochemistry of ilmenite megacrysts from the Monastery kimberlite, South Africa. Lithos, 29, 1–18.

Nakamura Y., Fujimaki K., Nakamura N. and Tatsumoto M. (1986)
Hf, Zr, and REE partition coefficients between ilmenite and liquid: Their inferences to lunar mare basalt petrogenesis. Journal of Geophysical Research, 91, D239–D250.

Neal C.R. (1986)
Kimberlite-like intrusives in the SW Pacific. Unpublished PhD thesis, University of Leeds (Leeds, UK), 327pp.

Neal C.R. and Davidson J.P. (1989)
An unmetasomatized source for the Malaitan alnöite (Solomon Islands): Petrogenesis involving zone refining, megacryst fractionation, and assimilation of oceanic lithosphere. Geochimica et Cosmochimica Acta, 53, 1975–1990.

Nixon P.H. and Boyd F.R. (1979)
Garnet bearing lherzolites and discrete nodule suites from Malaita alnöite, Solomon Islands, S.W. Pacific, and their bearing on oceanic mantle composition and geotherm. In: Boyd F.R. and Meyer H.O.A. (eds), The Mantle Sample. American Geophysical Union (Washington, DC), 400–423.

Ødegård M., Skår Ø., Schiellerup H. and Pearson N.J. (2005)
Preparation of a synthetic titanite glass calibration material for *in situ* microanalysis by direct fusion in graphite electrodes: A preliminary characterisation by EPMA and LA-ICP-MS. Geostandards and Geoanalytical Research, 29, 197–209.

Papike J.J., Hodges F.N., Bence A.E., Cameron M. and Rhodes J.M. (1976)
Mare basalts: Crystal chemistry, mineralogy and petrology. Reviews of Geophysics and Space Physics, 14, 475–540.

Pearce N.J.G., Perkins W.T., Westgate J.A., Gorton M.P., Jackson S.E., Neal C.R. and Chenery S.P. (1997)
A compilation of new and published major and trace element data for NIST SRM 610 and NIST SRM 612 glass reference materials. Geostandards Newsletter: The Journal of Geostandards and Geoanalysis, 21, 115–144.

Simonetti A. and Neal C.R. (2010)
In-situ chemical, U-Pb dating, and Hf isotope investigation of megacrystic zircons, Malaita (Solomon Islands): Evidence for multi-stage alkaline magmatic activity beneath the Ontong Java Plateau. Earth and Planetary Science Letters, 295, 251–261.

Stanin F.T. and Taylor L.A. (1979)
Armalcolite/ilmenite: Mineral chemistry, paragenesis, and origin of textures. Proceedings from the 10th Lunar and Planetary Science Conference, 383–405.

Warner R.D., Keil K., Muralli A.V. and Schmitt R.A. (1975)
Petrogenetic relationships among Apollo-17 mare basalts. In: Papers presented to the conference of the origins of mare basalts and their implications for lunar evolution. The Lunar Science Institute (Houston), 179–183.

Warner R.D., Taylor G.J., Keil K. and Planner H.N. (1978)
Green glass vitrophyre 78526: An impact melt of very low-Ti mare basalt composition. Proceedings of the 9th Lunar and Planetary Science Conference, 547–563.

